arXiv:1401.7754v3 [hep-ph] 1 Apr 2014

NNLO QCD corrections to Higgs pair production via vector boson fusion at hadron colliders

Ling Liu-Sheng, Zhang Ren-You, Ma Wen-Gan, Guo Lei, Li Wei-Hua, and Li Xiao-Zhou
Department of Modern Physics, University of Science and Technology of China (USTC),
Hefei, Anhui 230026, People's Republic of China

Abstract

The measurement of the Higgs pair production via vector boson fusion can be used to test the trilinear Higgs self-coupling and the $VVHH$ ($V = Z, W$) quartic gauge interactions. In this paper we present the calculations of the next-to-next-to-leading-order QCD corrections to the SM Higgs boson pair production via vector boson fusion at hadron colliders with the center-of-mass energy of 14, 33, and 100 TeV by using the structure function approach, and study the residual uncertainties from the factorization/renormalization scale, parton distribution functions and α_s on the total cross section. We also provide the distributions of transverse momenta, rapidities, invariant mass and azimuthal angle separations of final Higgs bosons. We observe a considerable quantitative reduction in the scale uncertainty due to the next-to-next-to-leading-order QCD corrections, and find that the total cross section is sensitive to the trilinear Higgs self-coupling.

PACS: 14.80.Bn, 12.38.Bx, 12.15.-y

1 Introduction

In the Standard Model (SM) and its extensions, the Higgs boson is responsible for the electroweak symmetry breaking (EWSB) and the generation of elementary particle masses. One of the primary goals of the LHC is to uncover the origin of EWSB and to determine whether a SM Higgs boson exists. A giant step was made recently; both the ATLAS and CMS collaborations have observed a new boson with the mass of ~ 126 GeV, and its properties are, so far, compatible with the SM Higgs [1]. The next important step is to investigate whether this particle is indeed responsible for the EWSB and, eventually, to determine whether it is really the SM Higgs boson. To do so, it is crucial to probe the Higgs self-interactions, since they trigger the EWSB and are indispensable to reconstruct the Higgs potential [2, 3, 4].

The Higgs pair production at hadron colliders is sensitive to the trilinear Higgs self-coupling. There are four main Higgs pair production channels: gluon-gluon fusion via top-quark loop, vector boson fusion (VBF), top-quark pair associated production and double Higgs-strahlung [5]. Among these Higgs pair production mechanisms, the gluon-gluon fusion mechanism provides the largest cross section, while the VBF mechanism yields the second largest cross section, which is quantitatively 1 order smaller than that via the former one. The VBF mechanism shows a clear experimental signature of two centrally produced Higgs bosons and two highly energetic forward/backward jets [6, 7], but the event analysis is still challenged by the smallness of its cross section [5, 8]. Therefore, a study of the VBF Higgs pair production can be feasible only at high luminosity and very high energy hadron colliders [9, 10]. At these hadron colliders, the Higgs pair production via weak vector boson fusion is not only the leading process, which is sensitive to the W^+W^-HH and $ZZHH$ interactions but also can be used to study the EWSB by probing trilinear Higgs self-coupling. In Ref.[11] Paolo Bolzoni *et al.* pointed out that the structure function approach [12] and the QCD factorization approximation work extremely well up to $\mathcal{O}(\alpha_s^2)$ corrections for the VBF processes, and the remaining contributions which are kinematically and parametrically suppressed, are practically negligible. The next-to-leading-order (NLO) and next-to-next-to-leading-order (NNLO) QCD corrections to the VBF single Higgs production at the LHC have been evaluated by using the structure function approach in

Refs. [11] and [12], separately.

In this work we present the calculations of the VBF Higgs pair production at hadron colliders with high luminosity or very high energy up to the QCD NNLO by using the structure function approach. The paper is organized as follows. In Sec. 2, we give a brief description of the structure function approach, and the strategy of the QCD NNLO calculation. The numerical results and discussion are presented in Sec. 3. A short summary is given in Sec. 4. In the Appendix the explicit expressions for coefficients C_{ij} $(i, j = 1, 2, 3)$ are provided.

2 Calculation setup

The structure function approach is a very good approximation to the VBF processes at hadron colliders, which is accurate at a precision level well above the typical residual scale and parton distribution function (PDF) uncertainties [11]. This approximation is based on the absence or smallness of the QCD interference between the two inclusive final proton remnants. The mechanism of the VBF Higgs pair production is analogous to the VBF single Higgs production. It can be viewed as the double deep-inelastic scattering (DIS) of two (anti)quarks with two virtual weak vector bosons independently emitted from the hadronic initial states fusing into a Higgs boson pair [8]. In particular, the interference between the Higgs pair radiated off the fusing weak vector bosons and the double Higgs-strahlung process via $qq' \to HHV^* \to HHqq'$ is negligible, and therefore the latter process is treated separately. Furthermore, the VBF Higgs pair production event can be easily selected because it includes two widely separated jets with high invariant mass. Therefore, we can use the structure function approach to provide the precision predictions at the QCD NNLO accuracy for the VBF Higgs pair production process at hadron colliders as used in the calculations for the VBF single Higgs production. The Feynman diagrams for the VBF Higgs pair production in proton-proton collisions are depicted in Fig.1, where P_i $(i = 1, 2)$ denote the 4-momenta of the initial protons, the virtual vector boson V can be either W or Z, G stands for the Goldstone boson, and X_i $(i = 1, 2)$ are the proton remnants.

By applying the structure function approach, the cross section for the VBF Higgs pair production can be calculated by contracting the DIS hadronic tensor $W_{\mu\nu}$ with the matrix

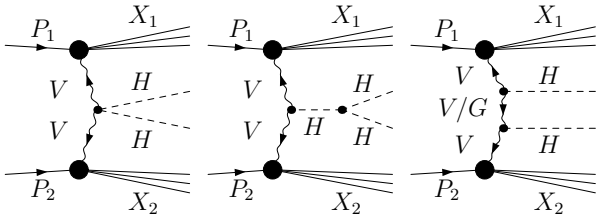

Figure 1: VBF Higgs pair production process at the hadron collider.

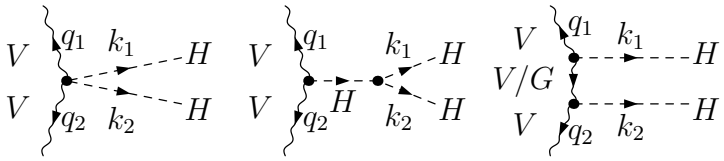

Figure 2: The Feynman diagrams for the $VV \to HH$ process.

element of the vector boson fusion subprocess $\mathcal{M}_V^{\mu\nu}$. The leading-order (LO) Feynman graphs for the $VV \to HH$ process are shown in Fig.2. The differential cross section for the VBF Higgs pair production process can be expressed as

$$d\sigma = \sum_{V=Z,W} d\sigma_V, \tag{1}$$

where

$$\begin{aligned} d\sigma_V &= \frac{G_F^2 M_V^4}{S(Q_1^2+M_V^2)^2(Q_2^2+M_V^2)^2} W_{\mu\nu}(x_1,Q_1^2)\mathcal{M}_V^{\mu\rho}\mathcal{M}_V^{*\nu\sigma}W_{\rho\sigma}(x_2,Q_2^2) \\ &\times \frac{d^3P_{X_1}}{(2\pi)^3 2E_{X_1}}\frac{d^3P_{X_2}}{(2\pi)^3 2E_{X_2}} ds_1 ds_2 \frac{d^3k_1}{(2\pi)^3 2E_1}\frac{d^3k_2}{(2\pi)^3 2E_2} \\ &\times (2\pi)^4\delta^4(P_1+P_2-P_{X_1}-P_{X_2}-k_1-k_2)\,. \end{aligned} \tag{2}$$

Here $d\sigma_V$ stands for the contribution of the VV $(V = Z, W)$ fusion process, G_F denotes the Fermi constant, S is the proton-proton colliding energy squared in the center-of-mass system (c.m.s), M_V is the mass of vector boson V, ${Q_i}^2 = -q_i^2$, and $x_i = {Q_i}^2/(2P_i \cdot q_i)$ are the usual DIS variables, and $s_i = (P_i + q_i)^2$ is the invariant mass squared of the i th proton remnant. By adopting the Feynman gauge, the matrix element of VV fusion subprocess can be expressed as

$$\begin{aligned} \mathcal{M}_V^{\mu\nu} &= 2\sqrt{2}G_F g^{\mu\nu}\left[\frac{2M_V^4}{(q_1+k_1)^2-M_V^2}+\frac{2M_V^4}{(q_1+k_2)^2-M_V^2}+\frac{6v\lambda_{HHH}^{SM}M_V^2}{(k_1+k_2)^2-M_H^2}+M_V^2\right] \\ &+\frac{\sqrt{2}G_F M_V^2}{(q_1+k_1)^2-M_V^2}(2k_1^\mu+q_1^\mu)(-k_1^\nu+k_2^\nu-q_1^\nu) \end{aligned}$$

$$+\frac{\sqrt{2}G_F M_V^2}{(q_1+k_2)^2-M_V^2}(2k_2^\mu+q_1^\mu)(k_1^\nu-k_2^\nu-q_1^\nu), \tag{3}$$

where M_V is the mass of W or Z, $\lambda_{HHH}^{SM}=\frac{M_H^2}{2v}$ is the SM trilinear Higgs self-coupling, and v is the vacuum expectation value of Higgs field. The DIS hadronic tensor has the form as [13]

$$\begin{aligned} W_{\mu\nu}\left(x_i,Q_i^2\right) &= \left(-g_{\mu\nu}+\frac{q_{i\mu}q_{i\nu}}{q_i^2}\right)F_1(x_i,Q_i^2)+\frac{\hat{P}_{i\mu}\hat{P}_{i\nu}}{P_i\cdot q_i}F_2(x_i,Q_i^2) \\ &+ \mathrm{i}\epsilon_{\mu\nu\alpha\beta}\frac{P_i^\alpha q_i^\beta}{2P_i\cdot q_i}F_3(x_i,Q_i^2), \qquad (i=1,2), \end{aligned} \tag{4}$$

where $\hat{P}_i=P_i-\frac{P_i\cdot q_i}{q_i^2}q_i$ and $F_j\left(x_i,Q_i^2\right)(j=1,2,3)$ are the usual DIS structure functions of proton [14].

For the VBF Higgs pair production the interferences between the u and t channels with identical final quarks (e.g., $uu\to HHuu$), and between the processes with WW and ZZ fusions (e.g., $ud\to ZZ/WW\to HHud$) at the LO, NLO, and NNLO in QCD are normally nonfactorizable. These nonfactorizable contributions would make Eq.(1) being incorrect even at the LO. However, these interference effects are heavily suppressed by kinematics for the VBF Higgs pair production. We have calculated these interference contributions at the LO by applying FeynArts-3.7 and FormCalc-7.4 packages [15] and found that they contribute less than 0.01% to the total cross section. Therefore, it is reasonable to neglect these interference contributions in the QCD LO, NLO, and NNLO calculations. Apart from these interference effects, in the QCD NNLO calculation, the diagrams involving the exchange of gluon between the two quark lines are also nonfactorizable. The same as in the VBF single Higgs production case [16], this nonfactorizable correction at the QCD NNLO is negligible for the VBF Higgs pair production.

We express the matrix element squared as

$$W_{\mu\nu}\left(x_1,Q_1^2\right)M^{\mu\rho}M^{*\nu\sigma}W_{\rho\sigma}\left(x_2,Q_2^2\right) = \sum_{i,j=1}^{3}F_i\left(x_1,Q_1^2\right)F_j\left(x_2,Q_2^2\right)C_{ij}. \tag{5}$$

The explicit expressions for C_{ij} $(i,j=1,2,3)$ are collected in the Appendix. The explicit expressions for the DIS structure functions at the LO and NLO have been given in Refs.[6, 17], and the NNLO expressions can be found in Refs.[11, 16]. In general, the DIS structure functions are expressed as convolutions of the PDFs with the Wilson coefficient functions C_i $(i=1,2,3)$. There are a number of PDFs at the QCD NNLO accuracy available, e.g., ABM11 [18], CT10

[19], HERAPDF1.5 [20], MSTW2008 [21], and NNPDF2.3 [22]. The Wilson coefficients can be obtained up to the QCD NNLO from Refs.[23, 24, 25], and the accurate parametrization of them can be taken from Ref.[26]. We developed a Fortran program to evaluate the numerical results for the VBF Higgs pair production process by employing the structure function approach. To verify the correctness of our calculations, we use our Fortran code to calculate the VBF Higgs pair production process at the QCD NLO accuracy by taking the same conditions as in Ref.[8], i.e., adopting the structure function approach and the MSTW2008 (90% C.L.) PDFs, setting $\mu = \mu_f = \mu_r = Q$, $M_H = 125$ GeV, and the other parameters being also the same as in Ref.[8]. Our numerical results of the total cross section are in good agreement with those in Table 3 of Ref.[8] implemented in the VBFNLO code [27]; e.g., we get $\sigma^{NLO}_{qq'HH} = 2.009(1)\ fb$ at the $\sqrt{S} = 14$ TeV LHC, which is coincident with $\sigma^{NLO}_{qq'HH} = 2.01\ fb$ in Ref.[8].

3 Numerical results and discussion

In this section we present and discuss the numerical results with the corrections up to the NNLO in QCD to the VBF Higgs pair production at the $\sqrt{S} = 14$, 33, and 100 TeV proton-proton colliders. In further numerical calculations, we mainly use the MSTW2008 (68% C.L.) PDFs [21] with the default value of strong coupling constant required by the set, while in comparison of the results by adopting different PDFs, we use separately the ABM11, CT10, HERAPDF1.5, MSTW2008 (68% C.L.) and NNPDF2.3 PDFs. The related SM input parameters are taken as [13]

$$M_H = 126 \text{ GeV},\ M_W = 91.1876 \text{ GeV},\ \ M_Z = 80.385 \text{ GeV},\ \ G_F = 1.1663787 \times 10^{-5} \text{ GeV}^{-2}. \quad (6)$$

A cut of $Q_i^2 > 4$ GeV^2 has been applied in order to render the results in the perturbative regime.

3.1 Cross sections and uncertainties

To make a strict cross section comparison between the theoretical predictions and experimental results, we should assess thoroughly the uncertainties affecting the central predictions of the total cross sections. In this section, we will discuss three kinds of uncertainties: (1) the scale uncertainty, which is an estimate of the missing higher-order contributions in the perturbative

calculation; (2) the PDF uncertainty; and (3) the uncertainty related to the fitted value of the strong coupling constant $\alpha_s(M_Z^2)$ and the parametric uncertainties related to the experimental errors.

3.1.1 Cross sections and scale uncertainty

The theoretical prediction of the cross section depends on the factorization scale μ_f, which originates from the convolution of the perturbative partonic cross section with the nonperturbative PDFs, and the renormalization scale μ_r that comes from the running of α_s. An estimate of the missing higher-order corrections can be considered as the variation of the central cross section with respect to these two scales. For simplicity we take the factorization scale being equal to the renormalization scale, i.e., $\mu = \mu_f = \mu_r$, and define $\mu = \kappa\mu_0$. We fix the central scale value as $\mu_0 = Q$ with μ varying in the range of $[0.25\mu_0,\ 4\mu_0]$. There, the central scale is the virtuality of the vector bosons which fuse into the Higgs boson pair. That is the most natural central scale choice for VBF processes [11]. In Figs.3(a,b,c), we depict the scale dependence of the integrated cross section for the VBF Higgs pair production process at the $\sqrt{S} = 14$, 33, and 100 TeV hadron colliders, separately, by using the MSTW2008 (68% C.L.) PDFs. If we define the scale uncertainty quantitatively as

$$\zeta \equiv \frac{max[\sigma(\mu)] - min[\sigma(\mu)]}{\sigma(\mu_0)}, \quad (\mu \in [1/4\mu_0, 4\mu_0]), \tag{7}$$

the scale uncertainty parameter ζ at the 14 TeV LHC can reach the value of 35% at the LO and is reduced to 3.9% by the NLO QCD corrections, while the NNLO scale uncertainty decreases to 2.3%. The LO, NLO, and NNLO scale uncertainties have the values of 15%, 6.3%, and 3.5% at the 33 TeV hadron collider and the values of 15%, 11.5%, and 5.9% at the 100 TeV hadron collider, respectively. We can see that the value of ζ at the QCD NNLO accuracy is less than the scale uncertainty of the NLO QCD corrected cross section at these hadron colliders.

Figure 4 shows the relative QCD corrections, δ_1 and δ_2, as functions of κ at the 14, 33, and 100 TeV hadron colliders by using the MSTW2008 (68% C.L.) PDFs, where we define $\delta_1 = \frac{(\sigma_{NLO}-\sigma_{LO})}{\sigma_{LO}}$ and $\delta_2 = \frac{(\sigma_{NNLO}-\sigma_{LO})}{\sigma_{LO}}$ to describe the relative NLO and NNLO QCD corrections separately. In Fig.4, the relative QCD corrections are obviously dependent on the value of κ;

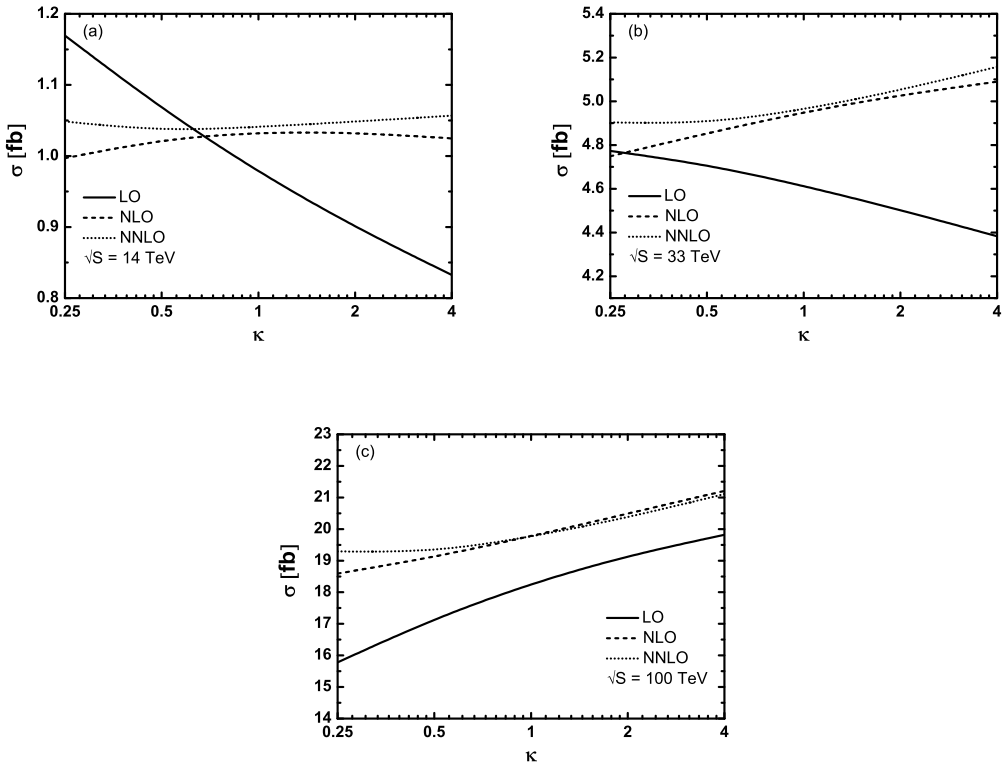

Figure 3: The scale dependence of the total cross section with $\mu = \kappa Q$ and $\kappa \in [1/4, 4]$ by using the MSTW2008 (68% C.L.) PDFs. (a) $\sqrt{S} = 14$ TeV. (b) $\sqrt{S} = 33$ TeV. (c)$\sqrt{S} = 100$ TeV.

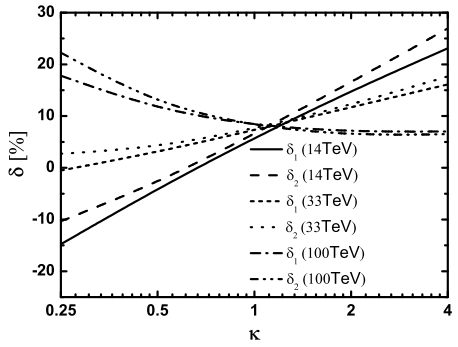

Figure 4: The relative QCD corrections, δ_1 and δ_2, as functions of κ at the $\sqrt{S} = 14$, 33, and 100 TeV hadron colliders with $\kappa \in [1/4, 4]$.

particularly, the curves for δ_1 are more intensively related to the scale than the corresponding δ_2 curves. We find that at the $\sqrt{S} = 14$ TeV LHC δ_1 and δ_2 are -15% and -9.0% at the position of $\kappa = 0.25$ but change to be 23% and 27% separately when $\kappa = 4$. Analogous to Fig. 3, the results concerning the relative corrections at the NNLO accuracy are less related to the renormalization and factorization scales than those at the NLO accuracy. That means the NNLO QCD corrections are very important in improving the scale uncertainty and make it possible to take full advantage of modern PDF sets at the same accuracy. We can also see from Fig.4 that at the position of the central scale ($\kappa = 1$) the relative corrections δ_1 and δ_2 are 6.4% and 6.9% at the $\sqrt{S} = 14$ TeV LHC and have the values of 6.8% (5.9%) and 7.2% (6.2%) at the $\sqrt{S} = 33$ (100) TeV hadron collider, respectively. These results show also the choice of $\kappa = 1$ can keep better convergence in the perturbative calculation than other values of κ. Therefore, we fix the scale $\mu = \mu_0$ in the following calculations unless stated otherwise.

In Table 1, we list the central values of the total cross section ($\kappa = 1$) and the errors due to scale uncertainty with κ varying in the range of $[1/4, 4]$ for the VBF Higgs pair production process at the LO, NLO, and NNLO by using the MSTW2008 (68% C.L.) PDFs. We can read from the table that the NNLO QCD corrected total cross section goes up from $1.986^{+0.045}_{-0}$ fb to $80.05^{+3.92}_{-0.80}$ fb as the increment of the hadron collider c.m.s. colliding energy $\sqrt{S}$ from 14 to 100 TeV, and the scale uncertainty of σ_{NNLO} is much smaller than the corresponding ones of σ_{LO} and σ_{NLO}. Therefore, we can see that from the point of view of improving the scale

$\sqrt{S}$	LO [fb]	NLO [fb]	NNLO [fb]
14 TeV	$1.858^{+0.374}_{-0.270}$	$1.976^{+0}_{-0.078}$	$1.986^{+0.045}_{-0}$
33 TeV	$11.234^{+0.878}_{-0.830}$	$12.002^{+0.190}_{-0.562}$	$12.041^{+0.359}_{-0.060}$
100 TeV	$75.36^{+4.91}_{-6.34}$	$79.82^{+3.92}_{-5.26}$	$80.05^{+3.92}_{-0.80}$

Table 1: The central values of the total cross section ($\kappa = 1$) and the errors due to scale uncertainty with $\kappa \in [1/4, 4]$ at the $\sqrt{S} = 14$, 33, and 100 TeV hadron colliders by using the MSTW2008 (68% C.L.) PDFs.

uncertainty the cross section prediction including the NNLO QCD corrections is more helpful for precision measurement of the VBF Higgs pair production process.

3.1.2 PDF and α_s uncertainties

Except the theoretical scale uncertainty, there is another source of theoretical uncertainty which is from the assumptions made on the parametrization of the PDFs. It is a pure theoretical error due to the parametrization choice, the set of input parameters used, the running of the parameters, etc. One way to quantify the pure theoretical uncertainties induced by these differences is to compare the predictions obtained with the various PDF sets, such as the ABM11 [18], CT10 [19], HERAPDF1.5 [20], MSTW2008 [21], and NNPDF2.3 [22] PDFs. In the calculations of the uncertainties from different PDF sets, the five files abm11_5n_nnlo.LHgrid, CT10nnlo.LHgrid, HERAPDF15NNLO_EIG.LHgrid, MSTW2008nnlo68cl.LHgrid, and NNPDF23_nnlo_as_0119.LHgrid are adopted.

Besides the differences between the various PDF sets, there are experimental uncertainties associated with the experimental data used to build the fit. The Hessian method is adopted by the ABM, CT10, HERA, and MSTW collaborations to estimate the PDF experimental uncertainty [21]. In this method, additional sets next to the best-fit PDF to account for the experimental uncertainties in the data are used to build the distribution functions. The NNPDF collaboration uses an alternative method to build the additional sets based on Monte Carlo replicas [28].

In addition to the PDF experimental uncertainty, there is also an uncertainty due to the errors on the value of α_s. The value of the strong coupling constant $\alpha_s(M_Z^2)$ is obtained by fitting the experimental data together with the parametric uncertainties related to the experimental

errors. That is the PDF α_s uncertainty due to the variation of the α_s value, which is sizeable and should be included in the total uncertainty. We evaluate the 68% C.L. α_s errors by taking $\Delta\alpha_s = \pm 0.0012$ [28, 29].

In Table 2, we list the NNLO QCD corrected total cross sections together with the PDF experimental uncertainty and α_s uncertainty at 68% C.L. obtained by adopting the ABM11, CT10, HERAPDF1.5, MSTW2008, and NNPDF2.3 PDF sets, separately. We can see that there are obvious discrepancies between the central values by using above five PDF sets. At the $\sqrt{S} = 14$ TeV (33, 100 TeV) hadron collider, the smallest central prediction is obtained from the NNPDF2.3 PDF set, which is about 3.2% (3.9%, 3.9%) smaller than the largest one predicted by adopting the ABM11 PDF set. In case with fixed colliding energy, the second largest central prediction is provided by the CT10 PDF set, which is about 2.2% larger than the smallest central prediction. The MSTW2008 PDF set provides the second smallest prediction at the $\sqrt{S} = 14$ TeV (33 TeV, 100 TeV) hadron collider. For each figure in this table, the first error is from PDF experimental uncertainty, and the second error is from α_s uncertainty. The data group obtained by adopting ABM11 PDFs shows about $\pm 1\%$ combined relative PDF $+\alpha_s$ uncertainty (i.e., PDF experimental relative uncertainty plus α_s relative uncertainty), and the other four data groups by adopting CT10, HERAPDF1.5, MSTW2008, and NNPDF2.3 PDFs show about $\pm(1.7 - 3.0)\%$ combined relative PDF $+\alpha_s$ uncertainties. The table shows clearly that the PDF experimental error is larger than the α_s error. For example, in the case of $\sqrt{S} = 14$ TeV, the MSTW2008 PDF experimental relative error is about $(+2.4\%/-1.7\%)$, while the α_s error is only $(+0.05\%/-0.05\%)$. However, the predictions of the total cross section with fixed $\sqrt{S}$ by adopting the CT10, HERAPDF1.5, MSTW2008, and NNPDF2.3 PDF sets are in agreement within the deviations from combined PDF experimental and α_s uncertainties at 68% C.L., except those obtained by using ABM11 PDFs. The total error of the total cross section can be figured out by adding linearly the scale and PDF $+\alpha_s$ uncertainties. According to the data in Table 1 and Table 2 which are obtained by using the MSTW2008 (68% C.L.) PDFs, we can get the total relative errors of the total cross section as $(+4.7\%/-1.8\%)$, $(+5.1\%/-2.2\%)$, and $(+6.9\%/-2.8\%)$ for the $\sqrt{S} = 14$ TeV, 33 and 100 TeV hadron colliders, separately.

PDF sets	$\sqrt{S} = 14\ TeV$ [fb]	$\sqrt{S} = 33\ TeV$ [fb]	$\sqrt{S} = 100\ TeV$ [fb]
ABM11	$2.048^{+0.020+0.003}_{-0.014-0.004}$	$12.475^{+0.113+0.038}_{-0.071-0.038}$	$83.20^{+0.68+0.259}_{-0.63-0.234}$
CT10	$2.023^{+0.039+0.001}_{-0.037-0.001}$	$12.255^{+0.210+0.022}_{-0.201-0.013}$	$81.74^{+1.28+0.255}_{-1.48-0.288}$
HERA1.5	$2.013^{+0.051+0.004}_{-0.044-0.006}$	$12.136^{+0.269+0.022}_{-0.232-0.030}$	$80.45^{+1.27+0.145}_{-1.41-0.159}$
MSTW2008	$1.986^{+0.047+0.001}_{-0.034-0.001}$	$12.041^{+0.240+0.018}_{-0.184-0.025}$	$80.05^{+1.33+0.246}_{-1.17-0.309}$
NNPDF2.3	$1.981^{+0.044+0.002}_{-0.045-0.007}$	$11.987^{+0.221+0.047}_{-0.249-0.080}$	$79.97^{+1.38+0.487}_{-1.67-0.749}$

Table 2: The NNLO QCD corrected total cross sections together with the 68% C.L. PDF experimental and PDF α_s uncertainties obtained by adopting the ABM11, CT10, HERAPDF1.5, MSTW2008 (68% C.L.) and NNPDF2.3 PDFs at the $\sqrt{S} = 14$ TeV, 33 and 100 TeV hadron colliders. For each result, the first error is from the PDF experimental uncertainty, and the second error is due to the α_s uncertainty.

3.2 Trilinear Higgs self-coupling

The SM Higgs potential can be written as

$$V(\Phi) = \lambda(\Phi^\dagger\Phi)^2 - \frac{1}{2}M_H^2\Phi^\dagger\Phi, \tag{8}$$

where

$$\Phi = \begin{pmatrix} G^+ \\ \frac{v+H+iG}{\sqrt{2}} \end{pmatrix}, \tag{9}$$

and G^+ and G are charged and neutral Goldstone bosons. We can rewrite the Higgs potential Eq.(8) in terms of Higgs field H as

$$V(H) = \frac{1}{2}M_H^2H^2 + \lambda vH^3 + \frac{\lambda}{4}H^4, \tag{10}$$

where the Higgs vacuum expectation value $v = \sqrt{\frac{M_H^2}{2\lambda}}$. Then, the SM trilinear Higgs self-coupling $\lambda_{HHH}^{SM} = \lambda v = \frac{M_H^2}{2v}$.

We deviate the trilinear Higgs self-coupling from its SM value by substituting $\lambda_{HHH}(= \eta\lambda_{HHH}^{SM})$ for λ_{HHH}^{SM} to study the sensitivity of the LO and NNLO QCD corrected total cross sections to the trilinear Higgs self-coupling strength by using the MSTW2008 (68% C.L.) PDFs. We find that both the LO and NNLO QCD corrected total cross sections are strongly dependent on the parameter η, as exemplified in Figs.5(a,b,c). There Figs.5(a), (b), and (c) are for the VBF Higgs pair production at the 14, 33, and 100 TeV hadron colliders, respectively. The corresponding K factors are shown in the lower plots of Figs.5(a,b,c). We see from the figures that the K factors are stable with the variations of parameter η.

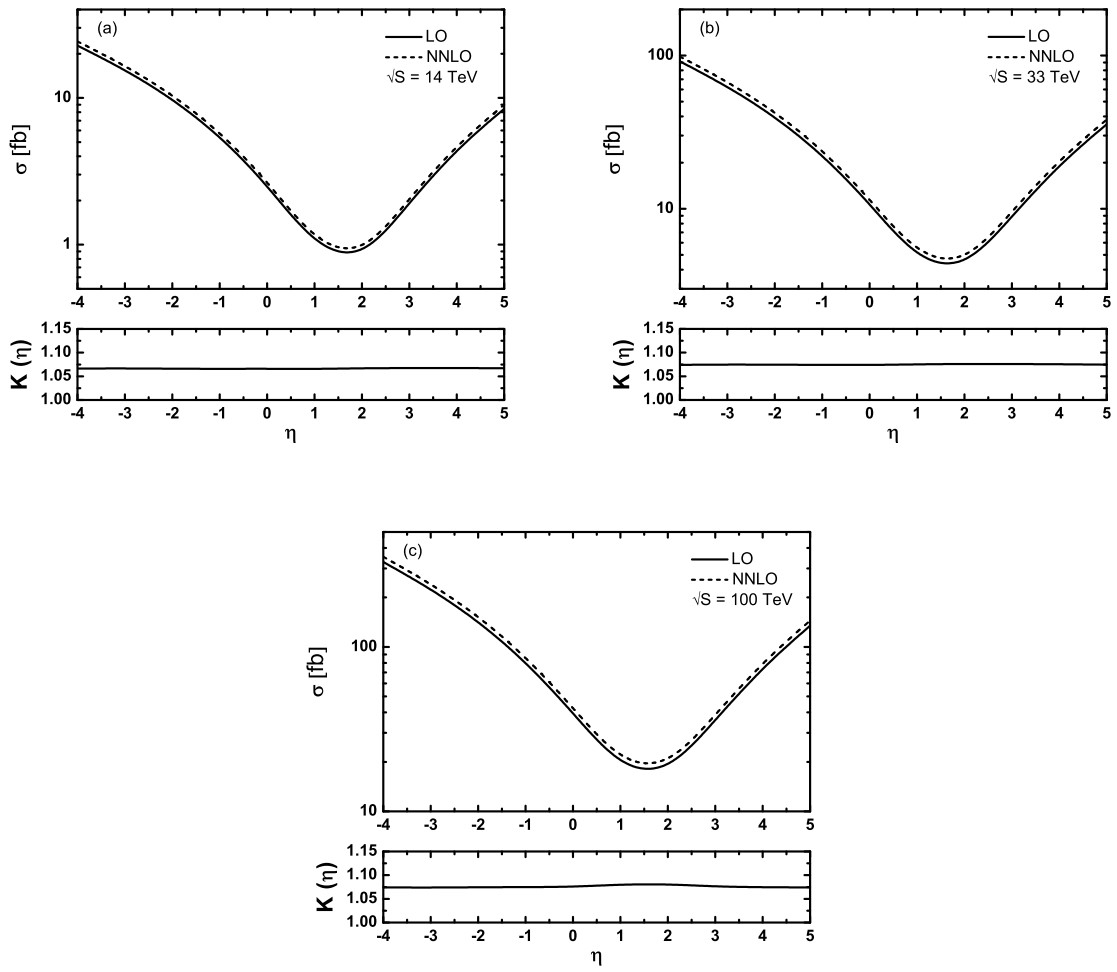

Figure 5: The LO and NNLO QCD corrected total cross sections and the corresponding K factors as functions of η by using the MSTW2008 (68% C.L.) PDFs where $\eta = \lambda_{HHH}/\lambda_{HHH}^{SM}$. (a) $\sqrt{S} = 14$ TeV. (b) $\sqrt{S} = 33$ TeV. (c)$\sqrt{S} = 100$ TeV.

3.3 Kinematic distributions

The signal of the VBF Higgs pair production is similar to the VBF single Higgs production. It involves two energetic forward/backward jets associated with two central Higgs bosons [6, 7]. This character plays an important role in discriminating the signal from the heavy QCD background. Since a precision study of the kinematic distributions of the final particles for the VBF Higgs pair production process is very helpful in the theoretical and experimental analyses, we provide the NNLO QCD corrected distributions of the transverse momenta (p_T) and the rapidities (y) for the final Higgs bosons, as well as the invariant mass (m_{HH}) and the azimuthal angle separations ($\Delta\phi$) of the final Higgs bosons. In the following, we call the Higgs boson with relatively larger transverse momentum among the final two Higgs bosons, i.e., $p_T^{H_1} > p_T^{H_2}$, as the first Higgs boson H_1 and the other Higgs boson as the second Higgs boson H_2.

By adopting the structure function approach, we can retain the differential information of final Higgs bosons up to QCD NNLO but obtain a rigorous description of final jets only at LO [30]. Therefore, we only provide the kinematic distributions for final Higgs bosons. The LO and NNLO QCD corrected transverse momentum distributions ($\frac{d\sigma_{LO}}{dp_T}$, $\frac{d\sigma_{NNLO}}{dp_T}$) and the corresponding K factors for the first Higgs boson at the 14, 33 and 100 TeV hadron colliders are shown in Figs.6(a,b,c), separately. Figs. 7(a,b,c) demonstrate the LO and NNLO QCD corrected p_T distributions and the corresponding K factors of the second Higgs at the $\sqrt{S} = 14$ TeV, 33 and 100 TeV hadron colliders, separately. We see from these six figures that the K factors of the NNLO QCD corrections are less than 1.10 in the plotted p_T range, and the p_T distributions of the first Higgs reach their maxima at the positions of $p_T \sim 90$, $p_T \sim 100$, and $p_T \sim 100$ GeV at the 14, 33, and 100 TeV hadron colliders, respectively, while the transverse momentum distributions of the second Higgs boson arrive their maxima at the position of $p_T \sim 50$ GeV at these three hadron colliders.

The LO and NNLO QCD corrected rapidity distributions and the corresponding K factors of the first Higgs and second Higgs boson by using the MSTW2008 (68% C.L.) PDFs are shown in Figs.8(a,b,c) and Figs.9(a,b,c), respectively. Figures 8(a) and 9(a) are for the 14 TeV LHC, Figs. 8(b) and 9(b) are for the 33 TeV hadron collider, and Figs. 8(c) and 9(c) are for the

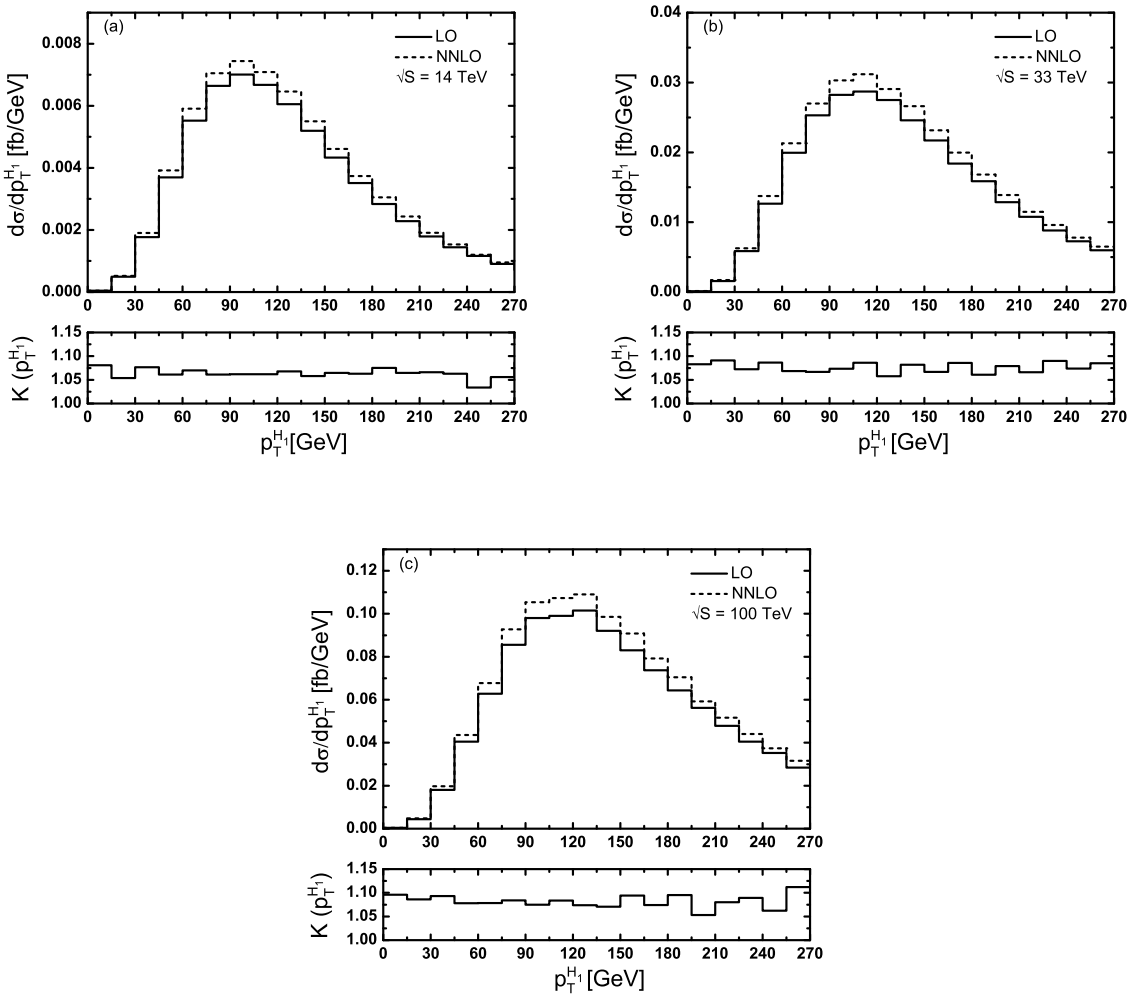

Figure 6: The LO and NNLO QCD corrected transverse momentum distributions and the corresponding K factors of the first Higgs boson ($p_T^{H_1}$) for the VBF Higgs pair production process by using the MSTW2008 (68% C.L.) PDFs. (a) $\sqrt{S} = 14$ TeV. (b) $\sqrt{S} = 33$ TeV. (c) $\sqrt{S} = 100$ TeV.

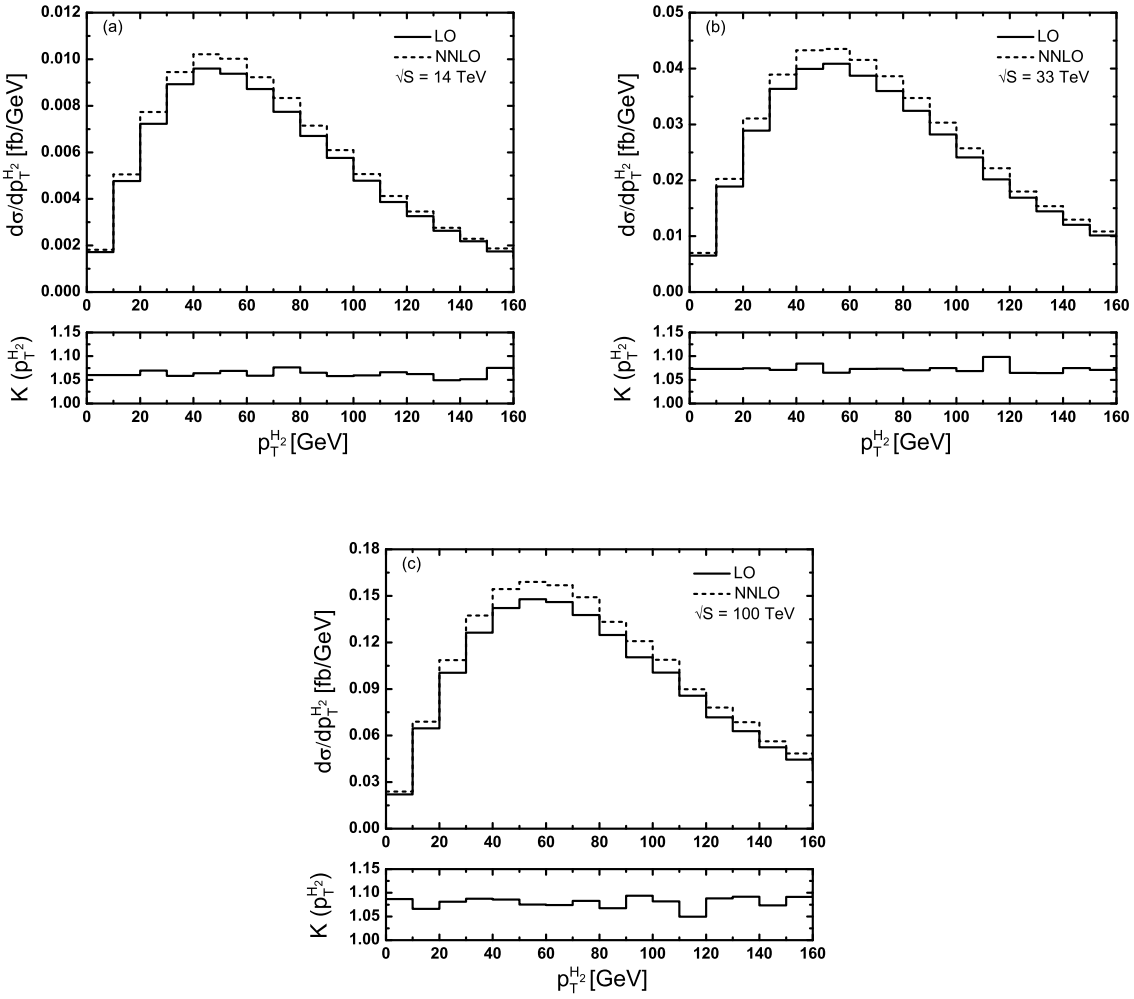

Figure 7: The LO and NNLO QCD corrected transverse momentum distributions and the corresponding K factors of the second Higgs boson ($p_T^{H_2}$) for the VBF Higgs pair production process by using the MSTW2008 (68% C.L.) PDFs. (a) $\sqrt{S} = 14$ TeV. (b) $\sqrt{S} = 33$ TeV. (c) $\sqrt{S} = 100$ TeV.

100 TeV hadron collider, separately. We can see that the two final Higgs bosons prefer to be produced in the central rapidity region with dozens of GeV transverse momentum (see Figs. 6 and 7 together). These characteristic distributions play an important role to discriminate the signal from the very heavy QCD background [6, 7].

In Figs. 10(a,b,c) we present the LO and NNLO QCD corrected distributions of the invariant mass of final Higgs boson pair (M_{HH}) and the corresponding K factors by using the MSTW2008 (68% C.L.) PDFs at the 14, 33, and 100 TeV hadron colliders, separately. From these figures, we see that for the VBF Higgs pair production at the hadron colliders the M_{HH} distributions are mostly concentrated in the vicinity of $M_{HH} \sim 400$ GeV and then decrease slowly with the increment of M_{HH}. The K factor varies from 1.05 to 1.10 in the plotted invariant mass range.

In Figs. 11(a,b,c) we present the LO and NNLO QCD corrected distributions of the azimuthal angle separation between the final two Higgs bosons ($\Delta\phi_{HH}$) and the corresponding K factors at the 14, 33, and 100 TeV hadron colliders, separately. There, we define the azimuthal angle separation $\Delta\phi_{HH} = |\phi_{H_1} - \phi_{H_2}|$, where ϕ_{H_1} and ϕ_{H_2} are the azimuthal angles of the Higgs boson H_1 and H_2. The plots show that the final two Higgs bosons prefer to be produced with large azimuthal angle separation, and the curves for K factors of the NNLO QCD corrections are almost independent of $\Delta\phi_{HH}$ in the plotted $\Delta\phi_{HH}$ range with the values less than 1.10 at the three hadron colliders.

4 Summary

Probing the Higgs self-interactions is extremely significant in understanding the EWSB mechanism. The VBF Higgs boson pair production is an important channel in studying the trilinear Higgs self-coupling. In this work, we calculate the NNLO QCD corrections to the VBF SM Higgs boson pair production at the $\sqrt{S} = 14$, 33, and 100 TeV hadron colliders by using the structure function approach. We investigate the theoretical uncertainty from the higher-order effects by varying the renomalization/factorization scale in the range of $[Q/4,\ 4Q]$ and conclude that the total cross section at the QCD NNLO accuracy is very stable. We also study the uncertainties from the PDFs and α_s and find if we take the combined PDF and α_s uncertainties into account, the total cross section predictions at the QCD NNLO by adopting the CT10, HERAPDF1.5,

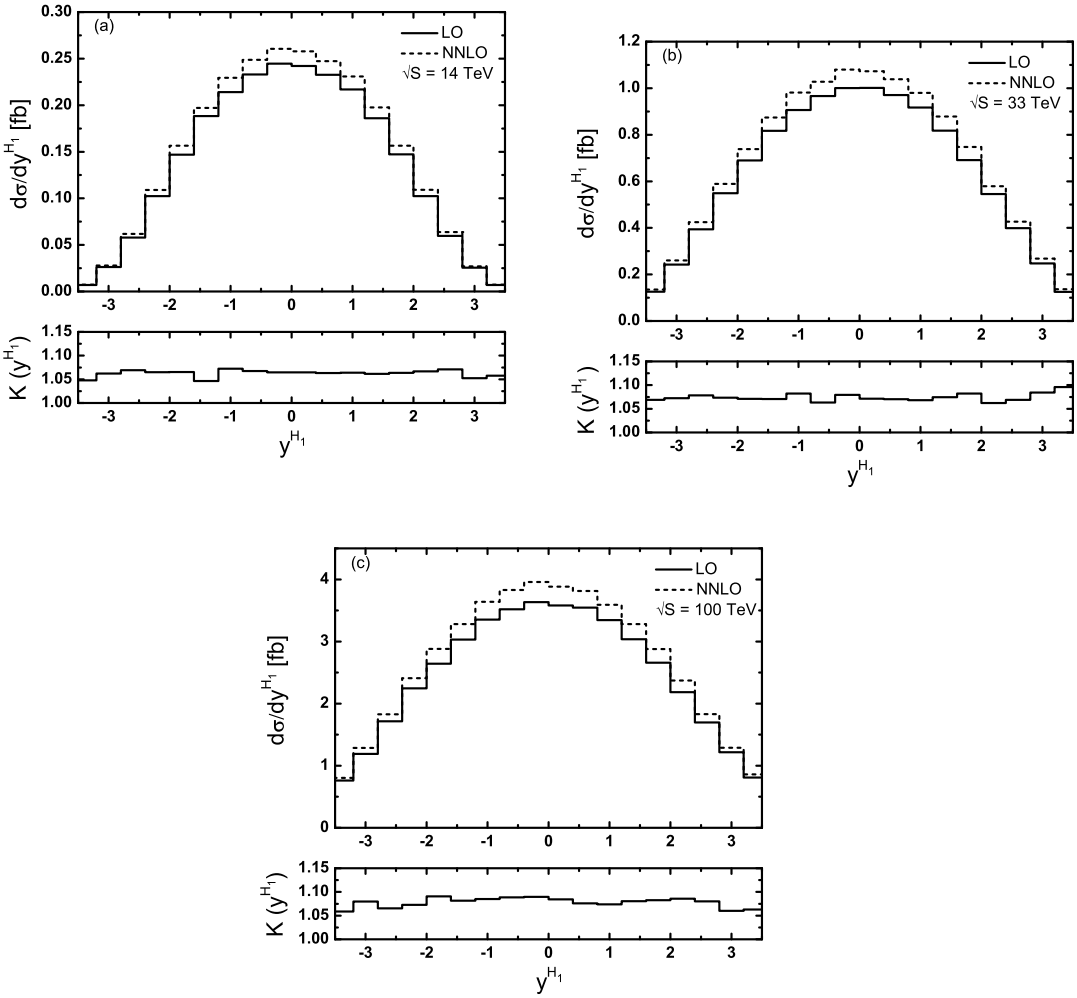

Figure 8: The LO and NNLO QCD corrected rapidity distributions and the corresponding K factors of the first Higgs (y^{H_1}) for the VBF Higgs pair production process by using the MSTW2008 (68% C.L.) PDFs. (a) $\sqrt{S} = 14$ TeV. (b) $\sqrt{S} = 33$ TeV. (c) $\sqrt{S} = 100$ TeV.

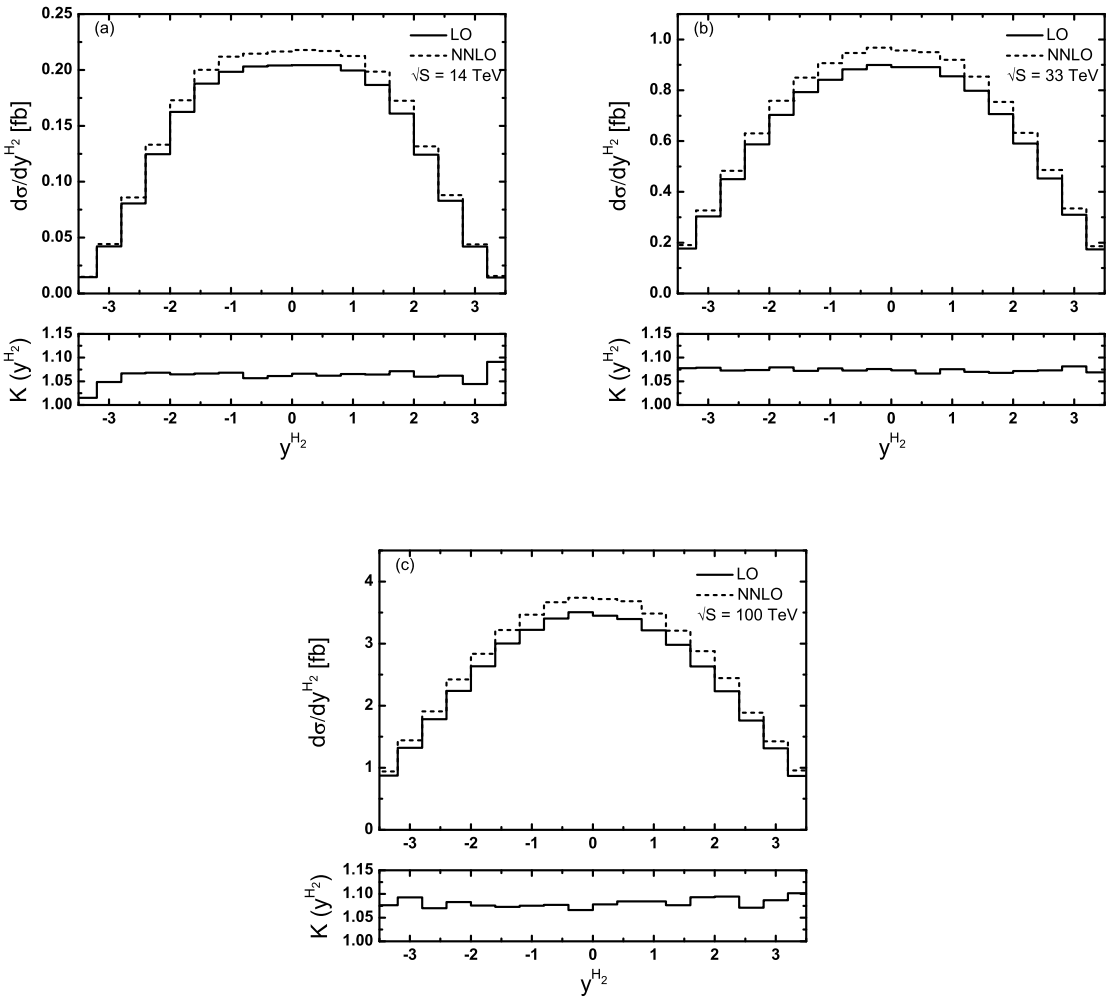

Figure 9: The LO and NNLO QCD corrected rapidity distributions and the corresponding K factors of the second Higgs (y^{H_2}) for the VBF Higgs pair production process by using the MSTW2008 (68% C.L.) PDFs. (a) $\sqrt{S} = 14$ TeV. (b) $\sqrt{S} = 33$ TeV. (c) $\sqrt{S} = 100$ TeV.

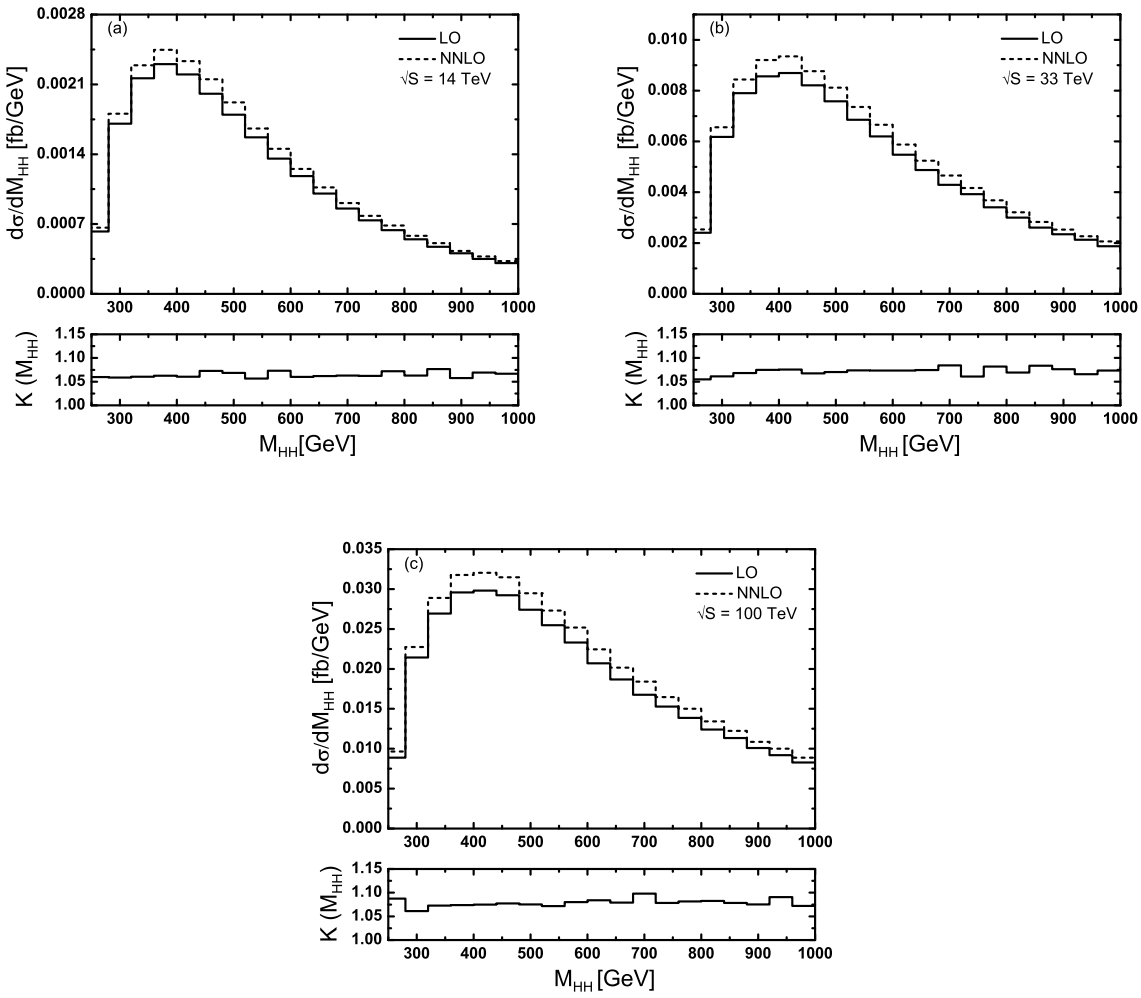

Figure 10: The LO and NNLO QCD corrected distributions of the Higgs pair invariant mass (M_{HH}) and the corresponding K factors for the VBF Higgs pair production process by using the MSTW2008 (68% C.L.) PDFs. (a) $\sqrt{S} = 14$ TeV. (b) $\sqrt{S} = 33$ TeV. (c) $\sqrt{S} = 100$ TeV.

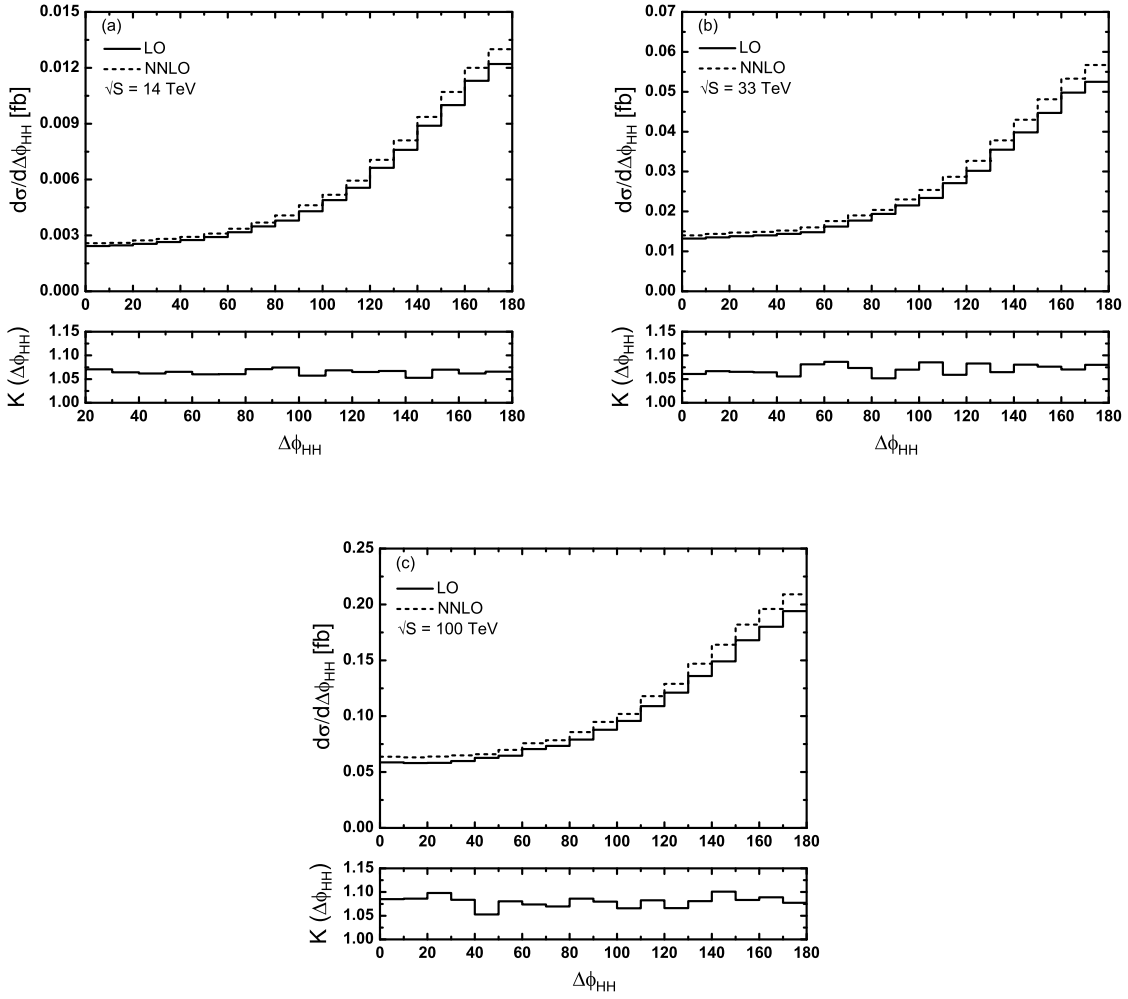

Figure 11: The LO and NNLO QCD corrected distributions of the azimuthal angle separation between the final two Higgs bosons ($\Delta\phi_{HH}$) and the corresponding K factors for the VBF Higgs pair production process by using the MSTW2008 (68% C.L.) PDFs. (a) $\sqrt{S} = 14$ TeV. (b) $\sqrt{S} = 33$ TeV. (c) $\sqrt{S} = 100$ TeV.

MSTW2008 (68% C.L.), and NNPDF2.3 PDF sets are in good agreement. We show also the sensitivity of the total cross section to the trilinear Higgs self-coupling and provide the distributions of the transverse momenta, rapidities, invariant mass, as well as the azimuthal angle separations of the final Higgs bosons.

Acknowledgments: This work was supported in part by the National Natural Science Foundation of China (Grants. No. 11275190, No. 11375008, and No. 11375171), and the Fundamental Research Funds for the Central Universities (Grant. No.WK2030040044). The numerical calculations were carried out in the Supercomputing Center of University of Science and Technology of China.

Appendix: Expressions for C_{ij}

By introducing the notations of

$$\begin{aligned}
A &= 2\sqrt{2}G_F\left[\frac{2M_V^4}{(q_1+k_1)^2-M_V^2}+\frac{2M_V^4}{(q_1+k_2)^2-M_V^2}+\frac{6v\lambda_{HHH}^{SM}M_V^2}{(k_1+k_2)^2-M_H^2}+M_V^2\right],\\
B &= \sqrt{2}G_F\frac{M_V^2}{(q_1+k_1)^2-M_V^2},\\
C &= \sqrt{2}G_F\frac{M_V^2}{(q_1+k_2)^2-M_V^2},
\end{aligned}$$

the coefficients C_{ij} appeared in Eq.(5) can be expressed as

$$\begin{aligned}
C_{11} &= \frac{1}{Q_1^2Q_2^2}\Big\{A^2\Big[(q_1\cdot q_2)^2+2Q_1^2Q_2^2\Big]+4AB\Big[Q_1^2Q_2^2(k_1\cdot k_2-M_H^2)\\
&+Q_2^2(q_1\cdot k_1)(q_1\cdot k_2-q_1\cdot k_1)\Big]-4AB(q_1\cdot q_2+q_2\cdot k_1-q_2\cdot k_2)\\
&\times\Big[(q_1\cdot k_1)(q_1\cdot q_2)+(q_2\cdot k_1)Q_1^2\Big]+4AC\Big[Q_1^2Q_2^2(k_1\cdot k_2-M_H^2)\\
&+Q_2^2(q_1\cdot k_2)(q_1\cdot k_1-q_1\cdot k_2)\Big]-4AC(q_1\cdot q_2-q_2\cdot k_1+q_2\cdot k_2)\\
&\times\Big[(q_1\cdot k_2)(q_1\cdot q_2)+(q_2\cdot k_2)Q_1^2\Big]+4B^2(q_1\cdot q_2+q_2\cdot k_1-q_2\cdot k_2)^2\\
&\times\Big[M_H^2Q_1^2+(q_1\cdot k_1)^2\Big]-4B^2Q_2^2\Big[M_H^2Q_1^2+(q_1\cdot k_1)^2\Big]\\
&\times\Big[2(k_1\cdot k_2-M_H^2-q_1\cdot k_1+q_1\cdot k_2)+Q_1^2\Big]+8BC\Big[(k_1\cdot k_2)Q_1^2+(q_1\cdot k_1)(q_1\cdot k_2)\Big]\\
&\times\Big[Q_2^2(2k_1\cdot k_2-2M_H^2-Q_1^2)+(q_1\cdot q_2)^2-(q_2\cdot k_1-q_2\cdot k_2)^2\Big]\\
&+4C^2(q_1\cdot q_2-q_2\cdot k_1+q_2\cdot k_2)^2\Big[M_H^2Q_1^2+(q_1\cdot k_2)^2\Big]
\end{aligned}$$

$$-4C^2Q_2^2\Big[M_H^2Q_1^2+(q_1\cdot k_2)^2\Big]\Big[2(k_1\cdot k_2-M_H^2+q_1\cdot k_1-q_1\cdot k_2)+Q_1^2\Big]\Big\},\qquad(11)$$

$$\begin{aligned}
C_{12} &= \frac{1}{(P_2\cdot q_2)Q_1^2Q_2^4}\Big\{-A^2\Big[(P_2\cdot q_1)^2Q_2^4+2(P_2\cdot q_1)(P_2\cdot q_2)(q_1\cdot q_2)Q_2^2\\
&+(P_2\cdot q_2)^2(q_1\cdot q_2)^2+Q_1^2Q_2^2(P_2\cdot q_2)^2\Big]+4AB\Big[Q_2^2(P_2\cdot k_1-P_2\cdot k_2+P_2\cdot q_1)\\
&+(P_2\cdot q_2)(q_1\cdot q_2+q_2\cdot k_1-q_2\cdot k_2)\Big]\Big[(P_2\cdot k_1)Q_1^2Q_2^2\\
&+(P_2\cdot q_1)(q_1\cdot k_1)Q_2^2+(P_2\cdot q_2)(q_1\cdot k_1)(q_1\cdot q_2)+(P_2\cdot q_2)(q_2\cdot k_1)Q_1^2\Big]\\
&+4AC\Big[Q_2^2(P_2\cdot k_2-P_2\cdot k_1+P_2\cdot q_1)+(P_2\cdot q_2)(q_1\cdot q_2-q_2\cdot k_1+q_2\cdot k_2)\Big]\\
&\times\Big[(P_2\cdot k_2)Q_1^2Q_2^2+(P_2\cdot q_1)(q_1\cdot k_2)Q_2^2+(P_2\cdot q_2)(q_1\cdot k_2)(q_1\cdot q_2)\\
&+(P_2\cdot q_2)(q_2\cdot k_2)Q_1^2\Big]-8BC\Big[(k_1\cdot k_2)Q_1^2+(q_1\cdot k_1)(q_1\cdot k_2)\Big]\\
&\times\Big[Q_2^2(P_2\cdot k_1-P_2\cdot k_2+P_2\cdot q_1)+(P_2\cdot q_2)(q_1\cdot q_2+q_2\cdot k_1-q_2\cdot k_2)\Big]\\
&\times\Big[Q_2^2(P_2\cdot k_2-P_2\cdot k_1+P_2\cdot q_1)+(P_2\cdot q_2)(q_1\cdot q_2-q_2\cdot k_1+q_2\cdot k_2)\Big]\\
&-4B\Big[M_H^2Q_1^2+(q_1\cdot k_1)^2\Big]\Big[Q_2^2(P_2\cdot k_1-P_2\cdot k_2+P_2\cdot q_1)\\
&+(P_2\cdot q_2)(q_1\cdot q_2+q_2\cdot k_1-q_2\cdot k_2)\Big]^2-4C^2\Big[M_H^2Q_1^2+(q_1\cdot k_2)^2\Big]\\
&\times\Big[Q_2^2(P_2\cdot k_2-P_2\cdot k_1+P_2\cdot q_1)+(P_2\cdot q_2)(q_1\cdot q_2-q_2\cdot k_1+q_2\cdot k_2)\Big]^2\Big\},
\end{aligned}\qquad(12)$$

$$C_{13} = 0,\qquad(13)$$

$$\begin{aligned}
C_{21} &= \frac{1}{(P_1\cdot q_1)Q_1^4Q_2^2}\Big\{-A^2(P_1\cdot q_1)^2Q_1^2Q_2^2-A^2\Big[(P_1\cdot q_1)(q_1\cdot q_2)+(P_1\cdot q_2)Q_1^2\Big]^2\\
&+4AB\Big[(P_1\cdot k_1)Q_1^2+(P_1\cdot q_1)(q_1\cdot k_1)\Big]\Big[Q_1^2Q_2^2(P_1\cdot k_1)-Q_1^2Q_2^2(P_1\cdot k_2)\\
&+Q_2^2(P_1\cdot q_1)(q_1\cdot k_1)-Q_2^2(P_1\cdot q_1)(q_1\cdot k_2)+(q_1\cdot q_2+q_2\cdot k_1-q_2\cdot k_2)(P_1\cdot q_1)(q_1\cdot q_2)\\
&+(q_1\cdot q_2+q_2\cdot k_1-q_2\cdot k_2)(P_1\cdot q_2)Q_1^2\Big]+4AC\Big[(P_1\cdot k_2)Q_1^2+(P_1\cdot q_1)(q_1\cdot k_2)\Big]\\
&\times\Big[Q_1^2Q_2^2(P_1\cdot k_2)-Q_1^2Q_2^2(P_1\cdot k_1)-Q_2^2(P_1\cdot q_1)(q_1\cdot k_1)+Q_2^2(P_1\cdot q_1)(q_1\cdot k_2)\\
&+(q_1\cdot q_2-q_2\cdot k_1+q_2\cdot k_2)(P_1\cdot q_1)(q_1\cdot q_2)+(q_1\cdot q_2-q_2\cdot k_1+q_2\cdot k_2)(P_1\cdot q_2)Q_1^2\Big]\\
&-4B^2\Big[(P_1\cdot k_1)Q_1^2+(P_1\cdot q_1)(q_1\cdot k_1)\Big]^2\Big[(q_1\cdot q_2+q_2\cdot k_1-q_2\cdot k_2)^2\\
&-2Q_2^2(k_1\cdot k_2-M_H^2-q_1\cdot k_1+q_1\cdot k_2)-Q_1^2Q_2^2\Big]+8BC\Big[(P_1\cdot k_1)Q_1^2\\
&+(P_1\cdot q_1)(q_1\cdot k_1)\Big]\Big[(P_1\cdot k_2)Q_1^2+(P_1\cdot q_1)(q_1\cdot k_2)\Big]\Big[Q_2^2(Q_1^2-2k_1\cdot k_2+2M_H^2)\\
&-(q_1\cdot q_2)^2+(q_2\cdot k_1-q_2\cdot k_2)^2\Big]-4C^2\Big[(P_1\cdot k_2)Q_1^2+(P_1\cdot q_1)(q_1\cdot k_2)\Big]^2\\
&\times\Big[(q_1\cdot q_2-q_2\cdot k_1+q_2\cdot k_2)^2-2Q_2^2(k_1\cdot k_2-M_H^2+q_1\cdot k_1-q_1\cdot k_2)-Q_1^2Q_2^2\Big]\Big\},
\end{aligned}\qquad(14)$$

$$
\begin{aligned}
C_{22} &= \frac{1}{4(P_1\cdot q_1)(P_2\cdot q_2)Q_1^4Q_2^4}\Big\{ -A\Big[2(P_1\cdot q_1)(P_2\cdot q_1)Q_2^2+2(P_1\cdot q_1)(P_2\cdot q_2)(q_1\cdot q_2)\\
&\quad +2(P_1\cdot q_2)(P_2\cdot q_2)Q_1^2+Q_1^2Q_2^2S\Big]+4B\Big[(P_1\cdot k_1)Q_1^2+(P_1\cdot q_1)(q_1\cdot k_1)\Big]\\
&\quad \times\Big[Q_2^2(P_2\cdot k_1-P_2\cdot k_2+P_2\cdot q_1)+(P_2\cdot q_2)(q_1\cdot q_2+q_2\cdot k_1-q_2\cdot k_2)\Big]\\
&\quad +4C\Big[(P_1\cdot k_2)Q_1^2+(P_1\cdot q_1)(q_1\cdot k_2)\Big]\Big[Q_2^2(P_2\cdot k_2-P_2\cdot k_1+P_2\cdot q_1)\\
&\quad +(P_2\cdot q_2)(q_1\cdot q_2-q_2\cdot k_1+q_2\cdot k_2)\Big]\Big\}^2, \qquad (15)\\
C_{23} &= 0, \qquad (16)\\
C_{31} &= 0, \qquad (17)\\
C_{32} &= 0, \qquad (18)\\
C_{33} &= \frac{1}{4(P_1\cdot q_1)(P_2\cdot q_2)}\Big\{A^2\Big[(q_1\cdot q_2)S-2(P_1\cdot q_2)(P_2\cdot q_1)\Big]-2AB\Big\{S\Big[-(k_1\cdot k_2)(q_1\cdot q_2)\\
&\quad +M_H^2(q_1\cdot q_2)+(q_1\cdot k_1)(q_1\cdot q_2)-(q_1\cdot k_1)(q_2\cdot k_1)+(q_1\cdot k_2)(q_2\cdot k_1)+(q_2\cdot k_1)Q_1^2\Big]\\
&\quad -2\Big[M_H^2(P_1\cdot q_2)(P_2\cdot q_1)-(k_1\cdot k_2)(P_1\cdot q_2)(P_2\cdot q_1)+(P_1\cdot k_1)(P_2\cdot k_1)(q_1\cdot q_2)\\
&\quad -(P_1\cdot k_1)(P_2\cdot q_1)(q_2\cdot k_1)-(P_1\cdot k_2)(P_2\cdot k_1)(q_1\cdot q_2)+(P_1\cdot k_2)(P_2\cdot q_1)(q_2\cdot k_1)\\
&\quad +(P_1\cdot q_1)(P_2\cdot k_1)(q_1\cdot q_2)-(P_1\cdot q_1)(P_2\cdot q_1)(q_2\cdot k_1)-(P_1\cdot q_2)(P_2\cdot k_1)(q_1\cdot k_1)\\
&\quad +(P_1\cdot q_2)(P_2\cdot k_1)(q_1\cdot k_2)+(P_1\cdot q_2)(P_2\cdot k_1)Q_1^2+(P_1\cdot q_2)(P_2\cdot q_1)(q_1\cdot k_1)\Big]\Big\}\\
&\quad -2AC\Big\{S\Big[M_H^2(q_1\cdot q_2)-(k_1\cdot k_2)(q_1\cdot q_2)+(q_1\cdot k_1)(q_2\cdot k_2)+(q_1\cdot k_2)(q_1\cdot q_2)\\
&\quad -(q_1\cdot k_2)(q_2\cdot k_2)+(q_2\cdot k_2)Q_1^2\Big]-2\Big[M_H^2(P_1\cdot q_2)(P_2\cdot q_1)\\
&\quad -(k_1\cdot k_2)(P_1\cdot q_2)(P_2\cdot q_1)-(P_1\cdot k_1)(P_2\cdot k_2)(q_1\cdot q_2)+(P_1\cdot k_1)(P_2\cdot q_1)(q_2\cdot k_2)\\
&\quad +(P_1\cdot k_2)(P_2\cdot k_2)(q_1\cdot q_2)-(P_1\cdot k_2)(P_2\cdot q_1)(q_2\cdot k_2)+(P_1\cdot q_1)(P_2\cdot k_2)(q_1\cdot q_2)\\
&\quad -(P_1\cdot q_1)(P_2\cdot q_1)(q_2\cdot k_2)+(P_1\cdot q_2)(P_2\cdot k_2)(q_1\cdot k_1)-(P_1\cdot q_2)(P_2\cdot k_2)(q_1\cdot k_2)\\
&\quad +(P_1\cdot q_2)(P_2\cdot k_2)Q_1^2+(P_1\cdot q_2)(P_2\cdot q_1)(q_1\cdot k_2)\Big]\Big\}+8BC\Big\{2(k_1\cdot k_2)\\
&\quad \times\Big[(P_1\cdot q_1)(q_1\cdot q_2)(P_2\cdot k_1+P_2\cdot k_2)-(P_1\cdot q_1)(P_2\cdot q_1)(q_2\cdot k_1+q_2\cdot k_2)\\
&\quad +Q_1^2(P_1\cdot q_2)(P_2\cdot k_1+P_2\cdot k_2)+(P_1\cdot q_2)(P_2\cdot q_1)(q_1\cdot k_1+q_1\cdot k_2)\Big]\\
&\quad -(k_1\cdot k_2)S\Big[(q_1\cdot q_2)(q_1\cdot k_1+q_1\cdot k_2)+Q_1^2(q_2\cdot k_1+q_2\cdot k_2)\Big]\\
&\quad -2M_H^2\Big[(P_1\cdot q_1)(q_1\cdot q_2)(P_2\cdot k_1+P_2\cdot k_2)-(P_1\cdot q_1)(P_2\cdot q_1)(q_2\cdot k_1+q_2\cdot k_2)\\
&\quad +(P_1\cdot q_2)Q_1^2(P_2\cdot k_1+P_2\cdot k_2)+(P_1\cdot q_2)(P_2\cdot q_1)(q_1\cdot k_1+q_1\cdot k_2)\Big]
\end{aligned}
$$

$$
\begin{aligned}
&+M_H^2 S\Big[(q_1\cdot q_2)(q_1\cdot k_1+q_1\cdot k_2)+Q_1^2(q_2\cdot k_1+q_2\cdot k_2)\Big]\\
&+2\Big[Q_1^2(P_1\cdot k_1-P_1\cdot k_2)(P_2\cdot k_2)(q_2\cdot k_1)-Q_1^2(P_1\cdot k_1-P_1\cdot k_2)(P_2\cdot k_1)(q_2\cdot k_2)\\
&-(P_1\cdot k_1)(P_2\cdot k_1)(q_1\cdot k_2)(q_1\cdot q_2)+(P_1\cdot k_1)(P_2\cdot k_2)(q_1\cdot k_1)(q_1\cdot q_2)\\
&-(P_1\cdot k_1)(P_2\cdot q_1)(q_1\cdot k_1)(q_2\cdot k_2)+(P_1\cdot k_1)(P_2\cdot q_1)(q_1\cdot k_2)(q_2\cdot k_1)\\
&+(P_1\cdot k_2)(P_2\cdot k_1)(q_1\cdot k_2)(q_1\cdot q_2)-(P_1\cdot k_2)(P_2\cdot k_2)(q_1\cdot k_1)(q_1\cdot q_2)\\
&+(P_1\cdot k_2)(P_2\cdot q_1)(q_1\cdot k_1)(q_2\cdot k_2)-(P_1\cdot k_2)(P_2\cdot q_1)(q_1\cdot k_2)(q_2\cdot k_1)\\
&-(P_1\cdot q_1)(P_2\cdot k_1)(q_1\cdot k_1)(q_2\cdot k_2)+(P_1\cdot q_1)(P_2\cdot k_1)(q_1\cdot k_2)(q_2\cdot k_2)\\
&+(P_1\cdot q_1)(P_2\cdot k_2)(q_1\cdot k_1)(q_2\cdot k_1)-(P_1\cdot q_1)(P_2\cdot k_2)(q_1\cdot k_2)(q_2\cdot k_1)\\
&-(P_1\cdot q_2)(P_2\cdot k_2)(q_1\cdot k_1)^2+(P_1\cdot q_2)(q_1\cdot k_2)(P_2\cdot k_2)(q_1\cdot k_1)\\
&+(P_1\cdot q_2)(q_1\cdot k_1)(P_2\cdot k_1)(q_1\cdot k_2)-(P_1\cdot q_2)(P_2\cdot k_1)(q_1\cdot k_2)^2\Big]\\
&+S\Big[(q_1\cdot k_1)-(q_1\cdot k_2)\Big]\Big[(q_1\cdot k_1)(q_2\cdot k_2)-(q_1\cdot k_2)(q_2\cdot k_1)\Big]\Big\}\Big\}. \qquad (19)
\end{aligned}
$$

References

[1] G. Aad, *et al.* (ATLAS Collaboration), Phys. Lett. B **716**, 1(2012); S. Chatrchyan *et al.* (CMS Collaboration), Phys. Lett. B **716**, 30(2012).

[2] D. D. Florian, J. Mazzitelli, Phys. Lett. B **724**, 306(2013).

[3] A. Papaefstathiou, L. L. Yang, J. Zurita, Phys. Rev. D **87**, 011301(2012).

[4] D. Y. Shao, C. S. Li, H. T. Li, and J. Wang, J.High Energy Phys. 07 (2013) 169.

[5] A. Djouadi, W. Kilian, M. Muhlleitner, P. M. Zerwas, Eur. Phys. J. C **10**, 45(1999); R. Frederix *et al.*, arXiv:1401.7340; M. J. Dolan, C. Englert, M. Spannowsky, J.High Energy Phys. 10 (**2012**) 112; A. J. Barr, M. J. Dolan, C. Englert, M. Spannowsky, Phys. Lett. B **728**, 308 (2014); M. J. Dolan, C. Englert, N. Greiner, M. Spannowsky, Phys. Rev. Lett. **112**, 101802 (2014); F. Goertz, A. Papaefstathiou, L.-L. Yang, J. Zurita, J.High Energy Phys. 06 (2013) 16.

[6] A. Djouadi, Phys. Rep. **457**, 1 (2008).

[7] D. Rainwater, Ph.D Thesis, University of Wisconsin - Madison, 1999.

[8] J. Baglio, A. Djouadi, R. Grober, M. M. Muhlleitner, J. Quevillon, M. Spira, J.High Energy Phys. 04 (**2013**) 151.

[9] http://hilumilhc.web.cern.ch/hilumilhc/index.html ; R. Assmann *et al.*, CERN-ATS-2010-177 (2010); E. Todesco and F. Zimmermann, *Proceedings of EuCARD-AccNet-EuroLumi Workshop: The High-Energy Large Hadron Collider*, Malta, Republic of Malta, 2010.

[10] G. Ambrosio, *et al.*, SLAC-R-591; FERMILAB-TM-2149F.

[11] P. Bolzoni, F. Maltoni, S.O. Moch, M. Zaro, Phys. Rev. Lett. **105**, 011801(2010).

[12] T. Han, G. Valencia, S. Willenbrock, Phys. Rev. Lett. **69**, 3274(1992).

[13] J.Beringer *et al.* (Particle Data Group), Phys. Rev. D **86**, 010001 (2012).

[14] A. De Roeck, R. S. Thorne, Prog. Part. Nucl. Phys. **66**, 727 (2011).

[15] T. Hahn, Comput. Phys. Commun. **140**, 418 (2001); T. Hahn, Proc. Sci. ACAT2010 (2010) 078.

[16] P. Bolzoni, F. Maltoni, S. O. Moch, M. Zaro, Phys. Rev. D **85**, 035002(2012).

[17] M. Spira, Fortschr. Phys. **46**, 203(1998).

[18] S.Alekhin *et al.*, Phys. Rev. D **86**, 054009 (2012).

[19] J. Gao, M. Guzzi, J. Huston, H. L. Lai, Z. Li, P. Nadolsky, J. Pumplin, D. Stump, C. P. Yuan, SMU-HEP-12-23.

[20] H1 and ZEUS Collaborations, arXiv:1107.4193.

[21] A.D. Martin, W.J. Stirling, R.S. Thorne, G. Watt, Eur. Phys. J. C **63**, 189(2009).

[22] R.D.Ball *et al.*, Nucl. Phys. B **876**, 244 (2013).

[23] S. Moch, J. A. M. Vermaseren, Nucl. Phys. B **573**, 853(2000).

[24] J. A. M. Vermaseren, A. Vogt, S. Moch, Nucl. Phys. B **724**, 3(2005).

[25] S. Moch, J. Vermaseren, A. Vogt, Nucl. Phys. B **813**, 220(2009).

[26] W. L. van Neerven, A. Vogt, Nucl. Phys. B **568**, 263(2000); W. L. van Neerven, A. Vogt, Nucl. Phys. B **588**, 345(2000).

[27] K. Arnold *et al.*, Comput.Phys.Commun. **180**, 1661 (2009).

[28] S. Alekhin *et al.*, arXiv:1101.0536.

[29] M. Botje *et al.*, arXiv:1101.0538.

[30] Marco Zaro and the VBF@NNLO collaboration, private communication.